Spring 2022

Stresses Within the Actin Meshwork Control the Turnover of Fimbrin During Clathrin-Mediated Endocytosis

Xiaobai Li
Yale University Graduate School of Arts and Sciences, xiaobai.li@yale.edu

Abstract

Stresses within the Actin Meshwork Control the Turnover of Fimbrin during Clathrin-mediated Endocytosis

Xiaobai Li

2022

In this dissertation, I investigated the molecular mechanism of clathrin-mediated endocytosis (CME) in fission yeast with a sparse labeling strategy to track endocytic proteins at the single molecule level. CME is involved in a variety of biological processes, such as nutrient internalization and receptor recycling. CME is also a well-conserved biological process from yeast to mammalian cells. During clathrin-mediated endocytosis, about 60 different endocytic proteins are recruited to the endocytic site in a highly reproducible order. During the endocytic event, endocytic proteins assemble into endocytic structures, contributing to membrane invagination and endocytic vesicle formation. Based on the single molecule endocytic protein trajectories I obtained, I proved the significance of stresses within the actin meshwork. I also investigated the dwell-time distribution of single molecules of fimbrin (a protein that crosslinks actin filaments) and provide new mechanisms for fimbrin-actin binding mechanism. To study the single-molecule endocytic protein dynamics, I upgraded a two-color Total Internal Reflection Fluorescence (TIRF) microscopy system to study the single molecule dynamics of endocytic proteins. The two-color imaging system can be applied to probe relative motions between endocytic proteins in further studies.

Stresses within the Actin Meshwork Control the Turnover of Fimbrin during Clathrin-mediated Endocytosis

A Dissertation

Presented to the Faculty of the Graduate School

Of

Yale University

in Candidacy for the Degree of

Doctor of Philosophy

By

Xiaobai Li

Dissertation Director: Julien Berro, PhD

May 2022

Table of Contents

Acknowledgement

First, I would like to express my deepest appreciation to my advisor, Professor Julien Berro. In my third year in graduate school, I joined Julien's lab and started a meaningful journey. Julien has always been supportive, providing insightful guidance with his expertise. Also, Julien is a great leader of research group, coordinating different projects among group members.

I would like to extend my gratitude to my committee, Professor Ziad Ganim and Sarah Slavoff for their helpful advice. In the past years, they have always been helping me with a better sense of the project, providing useful ideas and a lot of encouragement.

I would also like to thank all my current and previous lab mates in the past few years. I would like to thank Mike, Ronan, and Yuan for helping me with all kinds of biological topics. I would like to thank Rui and Iman for the discussions of different modeling and simulations. I would like to thank Qun and Barbara for helping with starin making and imaging. I really enjoyed working with all of you. Without any of you, I would not have made the current progress.

I would like to thank the Rothman lab, the Baddeley lab and the Lemon lab for the use of TIRF microscopes. I also want to thank Venkat, Satish, Kenny and Krishna for helping me with the use of microscopes.

I am grateful to thank my parents and grandparents. Without your support, I would not have been able to make it to this step. I am so proud of being the first person in the family submitting a dissertation at Yale University.

Last but not the least, I would like to thank my wife Zhe. Thanks to Yale chemistry admission board, we got to know each other in our first year in graduate school. My wife is a genius in every way that I could ever think of. It is my best luck to spend the rest of my life with you.

1 Introduction

1.1 Clathrin-mediated Endocytosis

Clathrin-mediated endocytosis (CME) is an essential and well-conserved process in eukaryotic cells[1–3]. It consists in the formation of small vesicles that internalize molecules from the plasma membrane and outside the cell into the cytoplasm[4,5]. In eukaryotic cells, since the plasma membrane is a barrier between the cell cytoplasm and the exterior environment, CME serves a significant role in transporting molecules into the cell interior for various purposes, such as nutrients uptake and recycling of receptors[6]. During CME in yeast, approximately 60 proteins are recruited in a highly reproducible temporal sequence[1,7]. Half of the endocytic proteins contribute to actin dynamics, which helps with producing the force necessary to shape the endocytic vesicle[8]. Specifically, CME generates vesicles of ~60-nm diameter[9] to transport cargo molecules into the cytoplasm. The whole process initiates with the formation of a membrane coat where the membrane coat proteins are recruited from the cytosol to the endocytic sites and cluster on plasma membrane[10–12]. The plasma membrane is then induced to invaginate and form a clathrin coated pit (CCP)[13]. Then, the invaginated membrane is pinched off at the neck to generate an endocytic vesicle separated from the plasma membrane inside the cell[14]. **Figure 1** illustrates the endocytic process with different stages. The endocytic structures are about 300nm in diameter[11] and the vesicle formation process happens within ~10s[10], which make it difficult to determine the precise temporal and spatial molecular organization of proteins during endocytic vesicle formation. In this work, we choose fission yeast (*Schizosaccharomyces pombe*) as model organism to study the endocytic

process. Fission yeast has relatively shorter doubling time (about 2.5hrs) compared to mammalian cells[15]. Also, fission yeast is a great model system because its genome can be edited rapidly and efficiently[16]. Most importantly, the endocytic proteins in fission yeast are highly conserved in other eukaryotic cells[2].

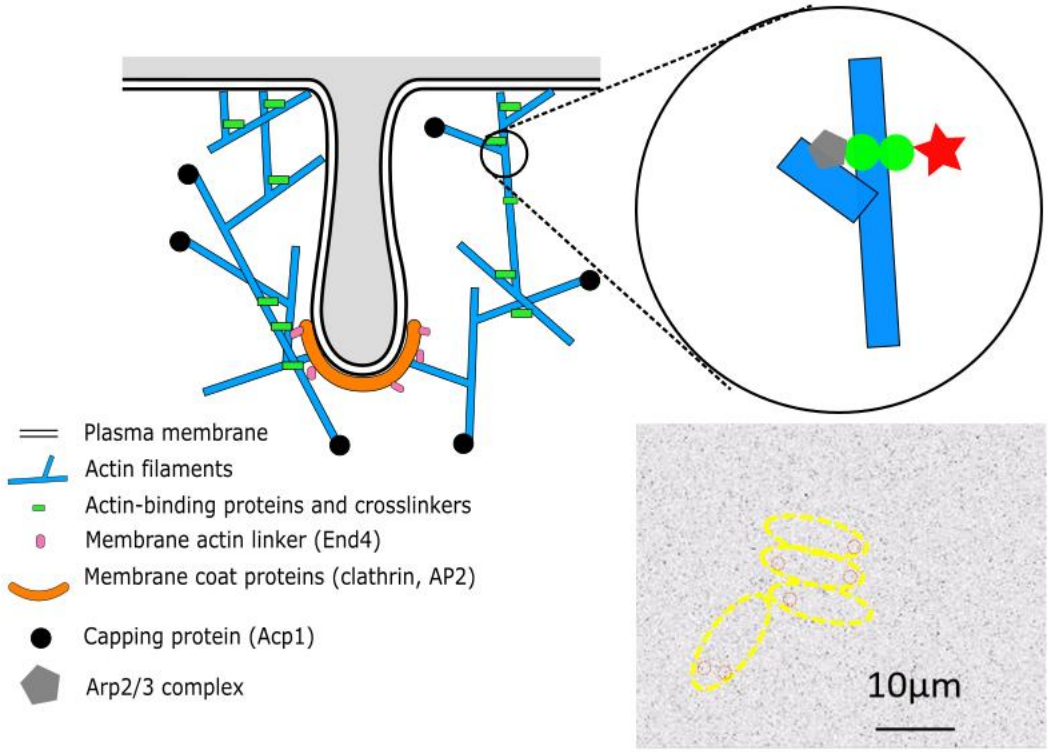

Figure adapted from *Lacy, et al*[17]

Figure 1. **Schematic of endocytic structures**

The left schematic includes endocytic proteins of interest: act1p, acp1p, fim1p, arp2/3 complex, end4p and clathrin. The top right shows the fim1p (green) labeled with SiR647 dye (red). The bottom right shows typical micrographs of fission yeast cells where fim1p was tagged and labeled for single-molecule study. Red circles show where the single molecule spots are.

1.2 Endocytic Proteins

The endocytic proteins can be categorized into three different groups: the membrane coat proteins, the actin meshwork related proteins and the scission proteins. Clathrin is a major component of the membrane coat. Clathrin assembles in clathrin triskelion to form a lattice[18]. For each clathrin triskelion, there are three clathrin heavy chains (chc1p) and three clathrin light chains (clc1p). The hexagonal and pentagonal clathrin lattice form the clathrin cage at the plasma membrane surface. During the formation of the clathrin coat, adaptor proteins are also recruited to the endocytic sites and link the clathrin coat and the actin meshwork to the membrane[7]. One example of adaptor protein in fission yeast is End4p, homologue of SLA2 in budding yeast and HIP1R in mammalian cells. *End4p* links the actin meshwork to the tip of the clathrin coated pit[19]. Adaptor proteins are also involved in the recruitment of clathrin and other endocytic protein to the endocytic sites[20].

Although several *in vitro* experiments showed that membrane can start to invaginate with only adaptor proteins[21], *in vivo,* the contribution of force from the actin meshwork is also needed to form an endocytic vesicle[8,22], which makes the whole process more complex. Since unlike in mammalian cells, yeast cells have cell walls and a high turgor pressure[22], it is hard for the membrane to invaginate. Under this scenario, the cell requires the contribution from actin meshwork assembly to provide extra force to help with the endocytic process. One evidence is that it has been shown by correlative fluorescence electron microscopy (CLEM) that the membrane invagination happens after the assembly of actin meshwork[23]. A schematic of actin meshwork can be found in **Figure 1**. Actin is the most abundant endocytic protein during endocytic process. It has

been shown that using drug Latrunculin A (LatA) to inhibit actin dynamics inhibits endocytic event. Treating yeast cells with 100μM LatA for 30min inhibits more than 90% of endocytic events[24]. Quantitative fluorescence microscopy has been utilized to show the motions of endocytic patches[25–27].

Some of other actin meshwork related proteins are also shown in **Figure 1**. During the assembly of the actin meshwork, actin monomers polymerize into actin filaments. New branches (daughter filaments) can be nucleated from existing actin filaments (mother filaments), requiring the activation of the Arp2/3 complex by the Wiskott-Aldrich Syndrome protein (WASp). The actin filament lengths are usually within the range of 100nm to 200nm[28]. To control the filament length, actin disassembly happens at the same time as polymerization by disassembly factors (such as ADF/Cofilin). In addition, actin capping proteins (the Acp1p/acp2p heterodimer in yeast) cap the growing barbed ends of actin filaments and stop their polymerization.

Within the actin meshwork, actin filaments are crosslinked by fimbrin (Fim1p)[29], which is the second most abundant protein during endocytosis[30]. It has been shown by multi-color TIRF that fimbrin bundles actin filaments in both parallel and antiparallel orientation[30]. It is also shown that fimbrin can bundle branched actin filaments with the absence of actin capping protein[31]. Fimbrin has three domains: a EH domain, which has an unknown function in endocytosis, and two actin binding domains (ABD1 and ABD2), which have homologous structures. *In vitro* experiments showed that actin filaments crosslinking of any one of the actin binding domains alone (ABD1 or ABD2) is less efficient than full-length fimbrin[31]. Although ABD2 alone has lower crosslinking efficiency, it significantly increases the actin polymerization rate *in vitro*[30]. It was also

found that fimbrin competes with other actin binding proteins, such as ADF/Cofilin, and excludes tropomyosin from actin patches[32–34].

Scission proteins are recruited to the endocytic site near the neck of membrane invaginations and are believed to participate in pinching off the vesicle at the late stage of endocytosis[35]. Unlike the endocytosis in mammalian cells, where dynamin is involved in membrane scission, dynamin is not necessary in endocytosis in fission yeast[27]. Hob1p and Hob3p are the amphiphysin and endophilin homologues in fission yeast that are involved in membrane scission.

1.3 Single Molecule Imaging in Yeast

Single molecule imaging of live yeast cells has always been challenging. One of the challenges is autofluorescence, which comes from the cellular background and overlay the signal from expected fluorophores. Another challenge specific to yeast cell imaging is the yeast cell wall, which prevents most of the organic synthetic dyes from entering the yeast cell[36]. However, single molecule imaging is still the best way to visualize the dynamics of molecules within submicrometric structures[37–39]. In the past decades, the development of labeling strategies, imaging techniques and data analysis tools have made it possible to image single molecule with live yeast cells[40].

1.3.1 Labeling Strategies

There are two different kinds of current common labeling strategies. One strategy is to edit the cell's genome to fuse a fluorescent protein to the protein of interest. Since genetically tagging proteins in yeast cells have been extensively performed for decades[41,42], fluorescent protein fusion is relatively easy and straightforward comparing

to doing so in other organisms. However, there are several disadvantages. For proteins with a high expression level, which is usually the case with endocytic proteins, fusing fluorescence proteins may end up with a large number of fluorophores close to each other. As a result, single molecule imaging cannot be achieved due to many fluorophores within one diffraction-limited spot. To deal with this problem, photoactivation localization microscopy (PALM) can be applied. For PALM, the activable fluorescent proteins can be switched on and off by an activation laser, where there is only a subpopulation of fluorophores activated at once[43]. In this case, better localization precision can be achieved.

Another problem with fluorescent proteins is the size. Since fluorescent proteins are relatively large, it may hinder the dynamics of the protein of interest after tagging. For example, tagging mEGFP on C-terminal of actin result in fission yeast growth defect[44,45]. Another drawback of fluorescent proteins is that their photostability and brightness are usually worse than synthetic organic dyes[46], which significantly affect the live cell single molecule imaging quality.

Using synthetic organic dyes has several advantages. They have better brightness and photostability compared to fluorescent proteins. They are in general smaller than fluorescent proteins, even if we account for the tag that can be used to specifically label proteins of interest, which makes them less likely to hinder the dynamics of the protein of interest. Also, synthetic organic dyes span a wider spectrum compared to the fluorescent proteins, making them the primary choice of yeast cells single molecule imaging. However, since yeast cells have a cell wall and several drug exporters, it is often more difficult for the synthetic dyes to enter and remain in yeast cells than for mammalian

cells. It has been reported that using electroporation can help with the internalization of synthetic dyes into yeast cells[47]. However, electroporation affects the cell morphology and its viability which is not a negligible factor to be considered. Another concern of synthetic organic dyes is the potential nonspecific binding, which requires optimization and proper controls before performing the actual experiment.

To image yeast cells with synthetic dyes, we need to fuse a protein tag to the protein of interest, which undergoes a self-labeling process to bind with the synthetic dyes. The most frequently used protein tags are CLIP[48]-, Halo-[49] and SNAP-Tags[50], which form covalent bonds with the synthetic dyes. The concentration of synthetic dyes can be tuned to achieve a desirable labeling efficiency, which makes it a most preferred choice for live cell single molecule imaging.

1.3.2 Imaging Techniques

The microscopy method plays an important role in yeast cell single-molecule imaging. To maximize the photon count for single-molecule imaging, wide-field illumination is preferred compared to confocal illumination[36]. The choice of imaging technique can also be dependent on the target that we want to image. For example, in our lab, total internal reflection Fluorescence (TIRF) microscopy (**Figure S1**) is the ideal technique[51,52] since our lab focuses on imaging single molecule dynamics of processes that happen on the cell plasma membrane, like endocytosis, and are close to the coverslip. In TIRF microscopy, the incident light travels to the interface between the cover slip and the sample with an incident angle larger than the critical angle, under which case there is no refraction but only reflection[53,54]. Since the cover slip and the sample have different

refractive index, an evanescent wave is generated at the interface penetrating through the sample[55]. The penetration length of the evanescent wave is typically shorter than 200nm for laser wavelengths typically used in biology[56]. As a result, the illumination is within 200nm from the cell wall and cell membrane, making it a perfect set up to image endocytic events. Since the illumination of TIRF microscopy is limited, we can avoid most of the background fluorescence, for example, the autofluorescence from fission yeast cell nucleus.

There are other imaging techniques utilized for single molecule imaging in yeast cells. For example, Highly Inclined and Laminated Optical Sheet (HILO) is extensively used in imaging the molecules in the cytoplasm or the nucleus[57]. In HILO, the incident angle is smaller than the critical angle, which leads to a larger penetration depth. For this reason, it is also called near-TIRF illumination. Although HILO has slightly worse signal-to-noise ratio compared to TIRF, its penetration depth can go up to about 3000nm, which is much larger than that in TIRF (about 200nm).

Narrow-field microscopy is another commonly used imaging technique for single molecule imaging. For narrow-field microscopy, the illumination focuses on a single cell to increase the illumination intensity. It allows fast imaging since higher illumination intensity leads to more photons emitted by fluorophores and thus shorter exposure time is required[58,59]. However, higher illumination intensity also leads to higher possibility of photodamage[60].

Light Sheet Fluorescence Microscopy (LSFM) is also a powerful technique that can be applied for single molecule imaging. LSFM projects a plane of light (light sheet) with one of the objectives to only illuminate a thin slice of the sample and use another

objective perpendicular to the first one to detect the fluorescence. It can avoid photodamage and achieve high signal-to-noise ratio[61,62]. However, if LFSM is used to image small sample as yeast cells, the two objectives could have steric hinderance relative to each other, making it difficult to focus[63,64]. Thus, LSFM is not considered to be a good single molecule imaging technique for yeast cells.

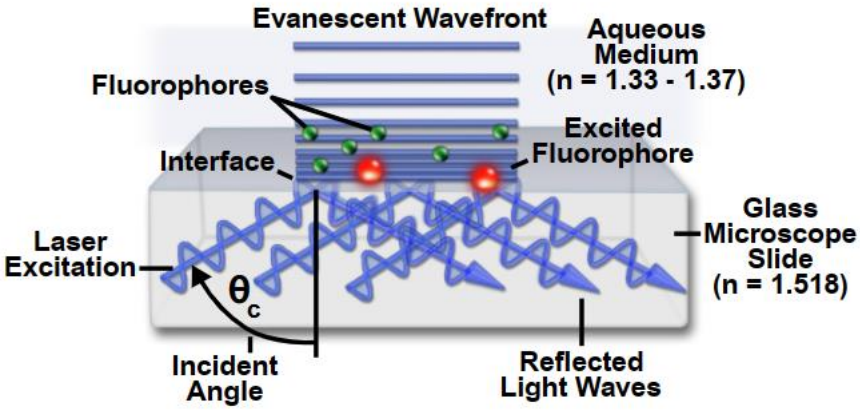

Figure S1. Schematic of total internal reflection fluorescence (TIRF) microscopy

Image adapt from MicroscopyU (https://www.microscopyu.com/techniques/fluorescence/total-internal-reflection-fluorescence-tirf-microscopy)

1.3.3 Data analysis

Another important component of single molecule imaging is data analysis. The first step in single molecule image data analysis is to determine the localization of each detected spot by fitting each spot with the 2D Gaussian distribution to denoise[65–68]. In this way, we can filter out the diffraction-limited spots withing the noise from different sources. After the detected spots are filtered, we need to find the same fluorophore detected in a series of consecutive frames and group them together. Several difficulties have made this step very challenging. One of the challenges is that the molecules are not only moving in the xy-plane, but also along the z-axis. For example, if we use TIRF microscopy to image the endocytic proteins during endocytic events, we usually set the focus to be near the bottom edge of the cell membrane, where the evanescent wave is generated. The endocytic structures span about 150 nm in length along the z-axis which indicates the range of the z-axis dynamics of endocytic proteins. Although the penetration length of the evanescent wave can be up to 200nm, since the evanescent wave field intensity decays exponentially as the penetration length increase[69], the imaging quality will decrease as the molecules moving along z-axis as well. There are several algorithms developed for single molecule imaging spots filtration and spots linking[70–73]. One of the commonly used algorithms is to first link the detected spots in consecutive frames into segmented tracks, which are then linked into trajectories later[36]. PYME[71] developed by David Baddeley is the software our lab used for single molecule image analysis. The details of imaging analysis with PYME can be found in **Methods and Experimental Design** section in this dissertation.

After the spot filtration and spot linking, we need to calculate the dynamics related quantities of single molecules of interest. One of the important quantities is mean squared displacement (MSD). By plotting MSD versus time interval, we can determine the type of diffusion and the diffusion constant[74,75].

It is possible that the trajectories of proteins we collected may consist of more than one type of diffusion. We could not simply fit the single molecule dwell-time distributions to an exponential function which indicates the molecule does not bind with a simple mass actin kinetics and its kinetics might contain multiple steps. However, directional motion is another possible component of the protein motion. In this case, a Hidden Markov Model (HMM) Bayesian Analysis can be applied to study different diffusion types within one trajectory[76–79].

1.4 Open Questions in the Field

In the past 30 years, researchers have identified about 60 kinds of endocytic proteins, figured out different stages during the endocytic process. More specifically, the order of recruitment of endocytic proteins and the specific endocytic event timeline have been extensively studied with various experimental approaches. However, there is still much unknown remaining, most of which are related to specific mechanisms at the nanometer scale. For example, it is known that the actin meshwork contributes to the production of the force required for membrane deformation, but the mechanisms of how the force is produced by the actin meshwork remains poorly understood. Since the yeast cells' turgor pressure is high, the amount of force needed for membrane invagination is higher than the amount of force the actin meshwork can produce based on the known

amount of actin molecules involved in endocytosis. In this thesis, I will illustrate the importance of stress within the actin meshwork and the mechanosensitive properties of the actin filament crosslinking protein fimbrin (Fim1p), which were not known before. Another unknown question is the relative motions of different endocytic proteins within the endocytic structures at the nanometer scale, which can help with understanding how different endocytic proteins are recruited and work together around endocytic sites. There are several technical difficulties: endocytic structures are smaller than the diffraction limit and membrane deformations linked to endocytic events happens within 10s. In this thesis, I will also explain the design of a two-color imaging system with total internal reflection fluorescence (TIRF) microscopy to measure the relative motions of endocytic proteins to endocytic sites.

2 Single Molecule Dwell-Time Distribution of Fimbrin Shows an Extra Peak

2.1 Background and Motivation

CME is an essential biological process conserved from yeast cells to mammalian cells. In fission yeast, the formation of a ~50nm-diameter endocytic vesicle takes about 20 seconds. However, how the endocytic proteins recruited to the endocytic site work together to shape a vesicle remains elusive. For example, theory predicts that 3000pN[80,81] force is needed to deform the yeast cell membrane during endocytic process and actin polymerization has been believed to be the source of the force needed. However, quantitative studies have determined that the number of actin filaments at endocytic site is smaller than 150, which is significantly not enough to produce 3000pN force by polymerization alone[82]. A better understanding of how the endocytic proteins contribute to the force production during endocytic events is needed. Since the whole process happens within a short time range and a length scale that is under diffraction limit, it is difficult to visualize the endocytic event using conventional fluorescence microscopy techniques.

Endocytic structures have been extensively studied with different microscopic techniques. Fluorescence recovery after photobleaching (FRAP) and Electron Microscopy (EM) data showed that the clathrin coat assembles on the flat membrane and induce the membrane invagination. Wide-field epifluorescence microscopy with a two-color dual-view add-on has been used to show the dynamics of endocytic patches during

membrane invagination and vesicle pinched off[25]. However, motions within the diffraction-limited endocytic patches could not be measured accurately.

Super-resolution imaging can also be applied to image endocytic structures. The idea of super-resolution is to take a time series of diffraction limited images and each image contains a few numbers of fluorophores. The position information of each detected fluorophore can be combined and reconstructed to the whole structure[83]. However, the dynamics of single-molecule endocytic protein have not been visualized due to the small size of endocytic proteins and their fast movements.

Our lab has developed a sparse labeling protocol which allows us to track single copies of endocytic proteins within the endocytic structures. Using this strategy, the lab tracked ten key endocytic proteins at single-molecule level and measured their dwell-time and their dynamics. It has been found that the average single-molecule endocytic protein dwell-time is less than 2 seconds for all the proteins tracked. However, the overall lifetime of endocytic protein in patches is between 20 seconds and 25 seconds[25], which indicates that endocytic proteins turn over rapidly during an endocytic event.

An interesting feature that brought to our notice is that the dwell-time distribution of fimbrin contains two peaks, where all other endocytic proteins dwell-time distribution only contains one peak. We hypothesized that the extra peak detected in fimbrin dwell-time distribution was from the force dependent unbinding between fimbrin and actin, which was suggested by the modeling work done by *Iman, et al*. We tested this hyphothesis in different ways illustrated in section 3.

2.2 Results

We applied single molecule tracking to the SNAP-SiR647[84] labeled fimbrin (Fim1p), actin (Act1p) and one subunit of the actin capping protein (Acp1p) (**Figure 2**). Fimbrin is a crosslinker of actin filaments. The capping protein binds to the barbed end of actin filaments to stop their polymerization. The dwell-time distribution of single molecule of Fim1p contained two peaks: one fast peak at ~0.5s and one slow peak at ~1.0s. The dwell-time distribution of single molecule Act1p and Acp1p both contained only one peak, which overlapped with the slow peak detected in Fim1p result. For all the protein of interested mentioned (Fim1p, Act1p, Acp1p), the dwell-time distributions had been measured by *Lacy, et al* with the same labeling and single molecule tracking method. Of all the proteins, the actin filament crosslinking protein was the only one whose dwell-time distribution contains two peaks.

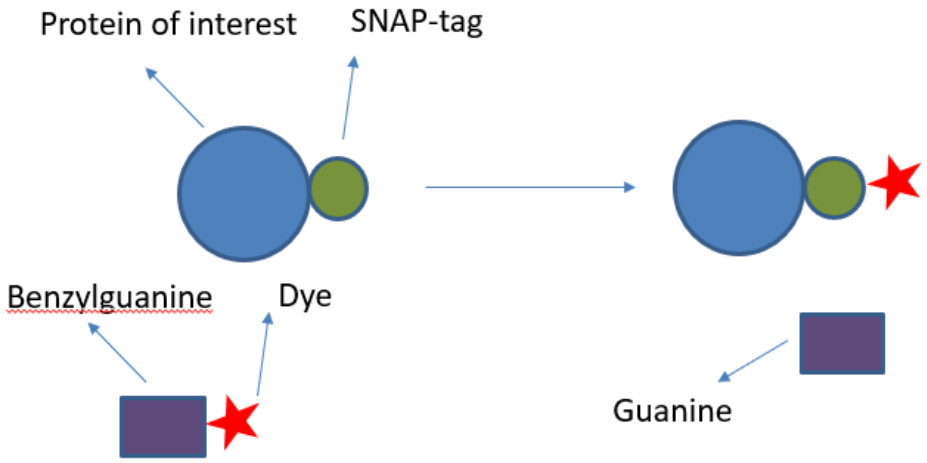

Figure S2. Schematic of binding between SNAP substrate and SNAP-tag

The dye binds to SNAP-tag with a covalent bond formation releasing Guanine.

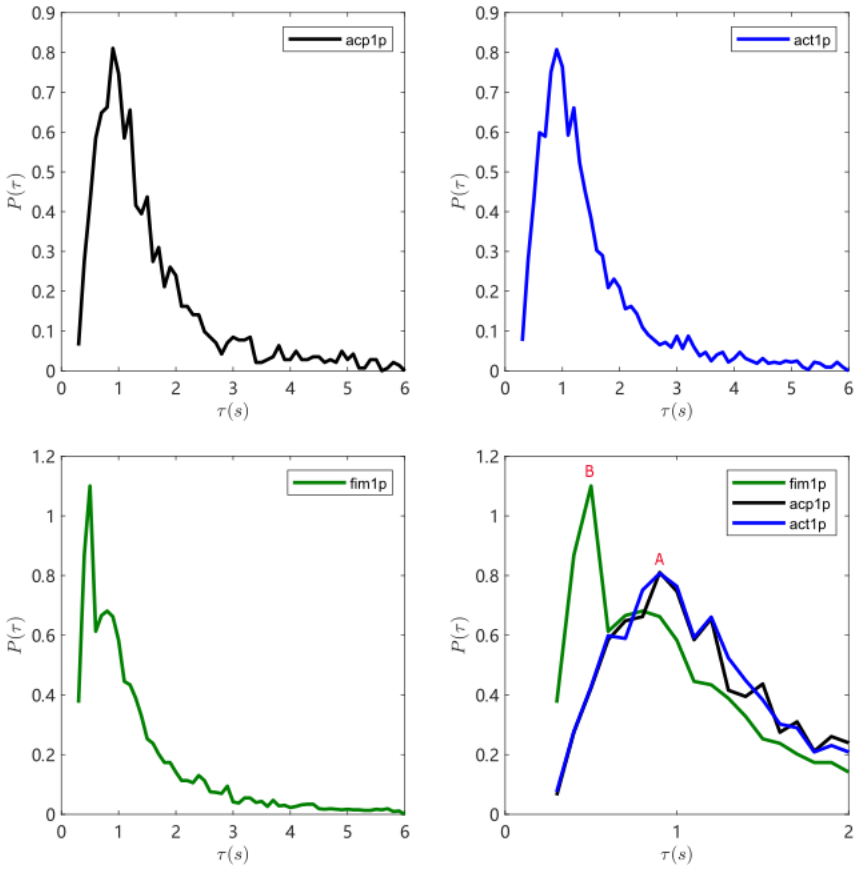

Figure 2. **The dwell-time distributions of acp1p, act1p and fim1p**

All three dwell-time distributions have a peak around 1 second, labeled as A, and referred to as the slow peak. The dwell-time distribution of fim1p has an extra peak around 0.5 second, labeled as B, and referred to as the fast peak.

The dwell-time distribution of acp1p contains 8577 tracks analyzed from 15 movies.

The dwell-time distribution of act1p contains 14283 tracks analyzed from 15 movies.

The dwell-time distribution of fim1p contains 21475 tracks analyzed from 25 movies.

3 Reducing the Stresses within the Actin Meshwork Results in the Disappearance of the Fast Peak

We would like to figure out where the two peaks detected in fim1p dwell-time distribution came from. We released the stresses within the actin meshwork to test if the unique peak detected in fim1p dwell-time distribution was due to the mechanical stresses in the endocytic actin meshwork. We first deleted the adaptor protein end4p, which linked the actin meshwork and the plasma membrane at the tip of the endocytic invagination. We found that the dwell-time distribution of fim1p in end4Δ cells (**Figure 3**) only had one peak that overlapped with the peak from dwell-time distribution of act1p and acp1p. The fast peak in the wild type fim1p dwell-time distribution disappeared when end4p was deleted. We then treated the cells with the latrunculin A (LatA) drug, which inhibits the polymerization of actin filaments. We then applied our single-molecule tracking strategy to fim1p in LatA treated cells (**Figure 4**). The fast peak present in fim1p dwell-time distribution in control conditions disappeared when cells were treated with LatA.

We also tried to split fim1p in half to release the stresses on fimbrin and within actin meshwork. We introduced the self-cleaving 2A peptide within the sequence of fim1p. The 2A peptide is a 20 amino-acid sequence that forces ribosomes to miss the formation of a covalent bond, therefore expressing the protein into two fragments in virtually the same quantity. Fim1p has three domains: a EH domain, which has an

unknown function, and two actin binding domains (ABD1 and ABD2). We made constructs to split fim1p at two different locations: 1) between the EF hand and ABD1 and 2) between ABD1 and ABD2. Since the SNAP tag was added at the C-terminus end of the Fim1p, we were able to determine the dwell-time distribution of ABD1-ABD2 or ABD2 (**Figure 5**). The dwell-time distribution of ABD1-ABD2 resembled the distribution we obtained for act1p, with only one peak at ~1.0s. Therefore, the EH domain was necessary for the second peak in fim1p dwell-time distribution. In contrast, the dwell-time distribution of ABD2 had a single peak at ~0.5s, which overlapped with the extra peak in the dwell-time distribution of full-length fim1p.

We proposed a working model to explain our data (**Figure 6**). The unbinding rate constant of ABD1 alone is slow, and essentially driven by actin disassembly. The unbinding rate constant of ABD2 alone, however, is fast. The unbinding of an ABD1-ABD2 construct would then be essentially driven by the unbinding of the slowest domain (ABD1). Because unbinding of ABD1 is slow, the disappearance of these constructs is driven by actin disassembly, which is much faster. However, the distribution of full length fimbrin looks like a combination of both ABD1 and ABD2 distributions. Since reducing the stress in the actin meshwork makes the extra peak of fimbrin dwell-time distribution disappear, we propose that the EH domain makes the slow ABD1 detachment rate faster, in a force dependent way. According to this model, the subpopulation of fimbrin under stress would essentially behave like ABD2 alone and another subpopulation not under stress would behave like ABD1 alone.

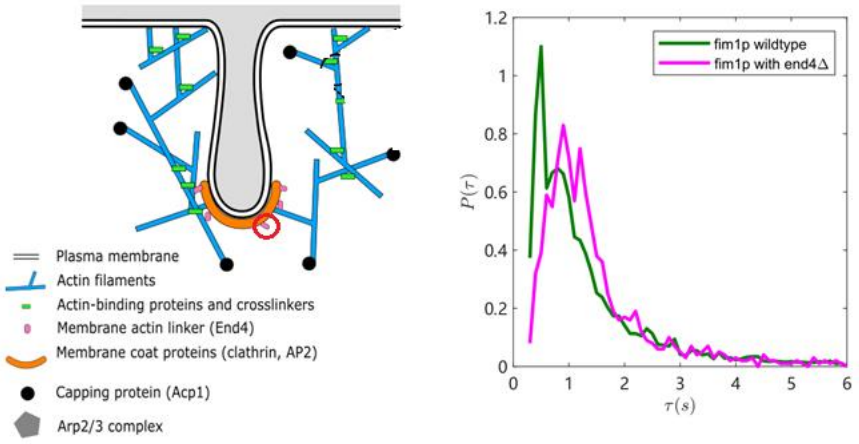

Figure 3. **Dwell-time distribution of Fim1p in wild type and *end4* Δ fission yeast cells**

The dwell-time distribution of Fim1p in wild type cells is shown in green. The dwell-time distribution of Fim1p in *end4*Δ is shown in magenta. End4p is the adaptor protein that links membrane to the actin meshwork, which is highlighted with red circle in the schematic on the left. In *end4*Δ cells, the dwell-time distribution of Fim1p only has one peak around 1 second.

The dwell-time distribution of Fim1p with end4Δ contains 6166 tracks analyzed from 15 movies.

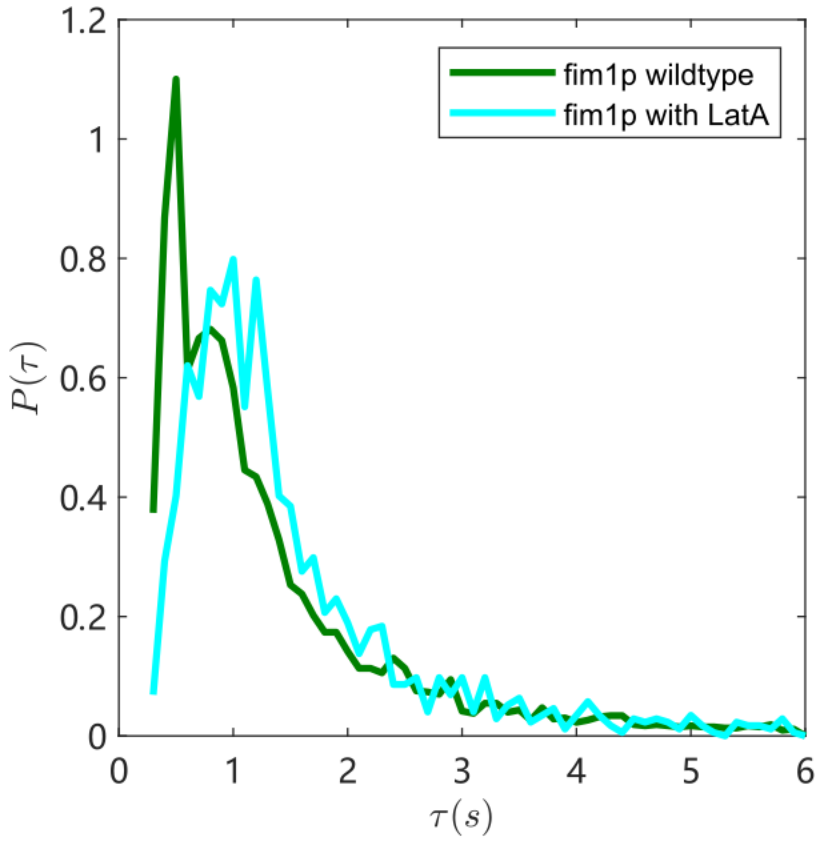

Figure 4. **Dwell-time distribution of fim1p in wild-type cells in control conditions and in the presence of Latrunculin A**

Fission yeast cells were treated with 100µm Latrunculin A (LatA) for 30 minutes. The dwell-time distribution of fim1p in wild-type cells is shown in green. The dwell-time distribution of fim1p in *end4*Δ is shown in cyan. In LatA treated cells, the dwell-time distribution of fim1p only has one peak around 1 second.

The dwell-time distribution of Fim1p with LatA treatment contains 7029 tracks analyzed from 15 movies.

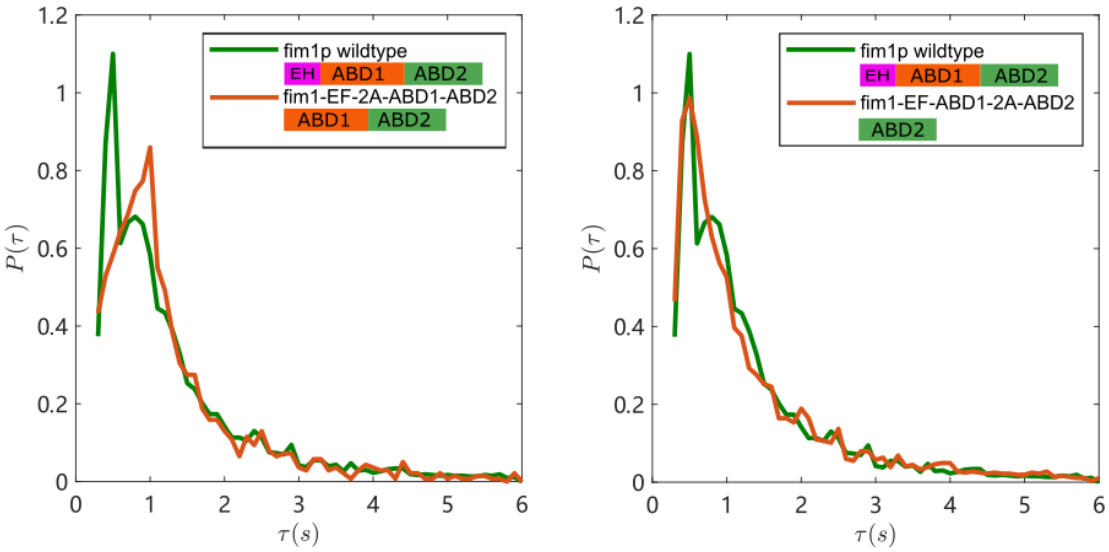

Figure 5. Dwell-time distribution of Fim1p mutants

The 20 amino-acid self-cleaving peptide sequence was genetically introduced into fim1p genome at two different locations. In the left figure, the self-cleaving peptide is between the EH and ABD1 domains. The ABD1-ABD2 construct has a single peak around 1 second. In the right panel, the self-cleaving peptide was introduced between the ABD1 and ABD2 domains. The dwell-time distribution of Fim1p ABD2 domain has a single peak around 0.5 second.

The dwell-time distribution of ABD1-ABD2 contains 8260 tracks analyzed from 15 movies.

The dwell-time distribution of ABD2 contains 6194 tracks analyzed from 15 movies.

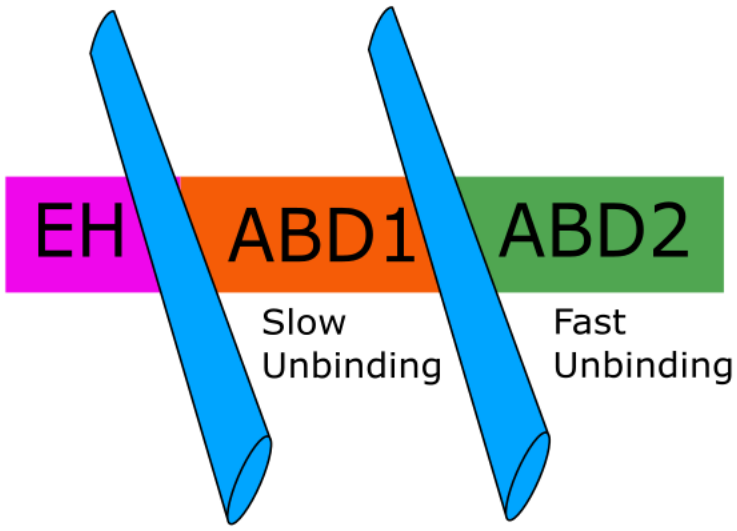

Figure 6. A working model for the crosslinking of actin filaments by fimbrin

Actin filaments are shown as blue rods. The model proposes that the unbinding rate constant of ABD1 alone is slow, and essentially driven by actin disassembly, whereas the unbinding rate constant of ABD2 alone is fast. The unbinding of an ABD1-ABD2 construct would then be essentially driven by the unbinding of the slowest domain (ABD1).

4 Visualizing the Single-Molecule Dynamics of Endocytic Proteins with Two-color TIRF Microscopy

4.1 Background and Motivation

Since the detailed mechanism of how endocytic proteins cooperate together to produce force during clathrin-mediated endocytosis is still elusive, we decided to build a two-color TIRF imaging system. Using two colors, we will be able to determine how proteins move relatively to each other within the endocytic structure and better understand how forces are produced. Our first plan was to image two endocytic proteins at single molecule level. However, since we sparsely label the proteins of interest, finding two spots of two different endocytic proteins at the same endocytic site has very low probability. Therefore, we decided to tag all the copies of one protein of interest with a fluorescent protein to locate the center of mass of this protein in the endocytic patch, and determine the movements of single-molecules of a second protein of interest relatively to this center of mass.

4.2 Results

The initial imaging system we used for two-color TIRF imaging is a single color TIRF microscope equipped with 555nm and 640nm laser. To do two-color imaging, we had to switch between two channels every 100ms. In this case, it is not the most suitable

way to visualize single molecule endocytic protein based on their known fast turn over behavior.

We imaged two different endocytic proteins with different labeling strategies. We imaged one protein of interest at single molecule level as described in previous chapters. The other protein of interest was labeled with a fluorescent protein. In this case, we can calculate the center of mass of the endocytic protein patch and use it to determine the relative movements of the first protein of interest relatively to the endocytic structure. To find out the most suitable labeling strategy, we tested several different fluorescent proteins for patch tracking with two-color TIRF system.

We started with the existing mCherry strains in our lab. We used a 561nm laser to excite mCherry and found that there are autofluorescence that cannot be filtered out (**Figure S3**). We also found bleed though between mCherry and SiR647 emission channels. For these reasons, we switched to using mEGFP. mEGFP has also better brightness than mCherry, which makes it a better candidate for our two-color imaging experiments. In addition, the emission profile of mEGFP is far from that of SiR647, which helps us to avoid bleed through artifacts. We also started to use a two-color TIRF microscope with Gemini W-view system, which allows us to image both fluorophores simultaneously with 488nm and 640nm laser. Also, there is no need to switch between channels every 100ms anymore.

In **Figure 7**, we present some preliminary results for imaging mEGFP-fim1 acp1-SNAP-SiR647 strain with two-color TIRF microscope. By illuminating the sample with the 488nm laser, we did not detect much bleed through into the SiR647 emission channel. By using both 488nm and 640nm laser, we could collect both patch and single molecule

information simultaneously. We have analyzed the spots detected in SiR647 channel and found that the dwell-time is comparable to what we obtained from single color TIRF imaging experiment (~1.5s). However, due to some software synchronization issues, we were not able to tune the 640nm laser intensity to achieve the best imaging quality. The labeling efficiency of SiR647 needs to be tuned to a lower level as well.

Instead of imaging fim1p patch, using myo1p patch could be a better choice. It has been shown that myo1p patch form a ring shape structure around the neck of CCP and remains at the plasma membrane after the vesicle is pinched off. Also, we imaged myo1p at single molecule level and calculated MSD. From the MSD plot of Myo1p (**Figure S4**), myo1p has a hindered motion in limited region compared to fim1p. For this reason, we can use myo1p-mEGFP as a good reference of the location of endocytic cite.

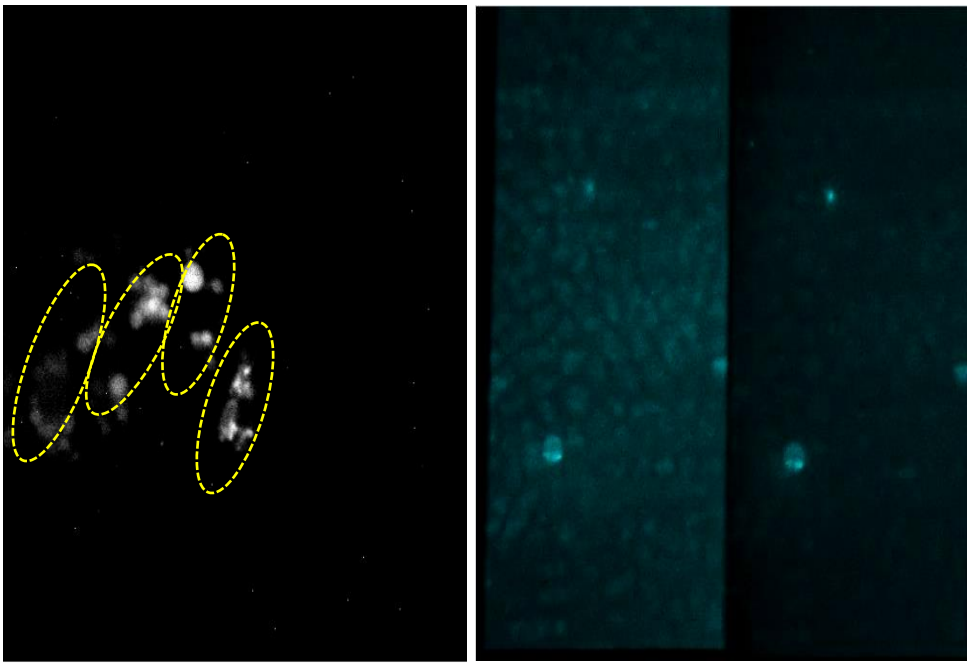

Figure S3. Myo1-mCherry strain imaged by two-color TIRF system

Left: myo1-mCherry strain imaged with 561nm laser. Right: myo1-mCherry strain imaged with 561nm laser and 647nm laser simultaneously. Autofluorescence can be detected from the background in the left figure. There is laser bleed through between mCherry and SiR emission channels.

A

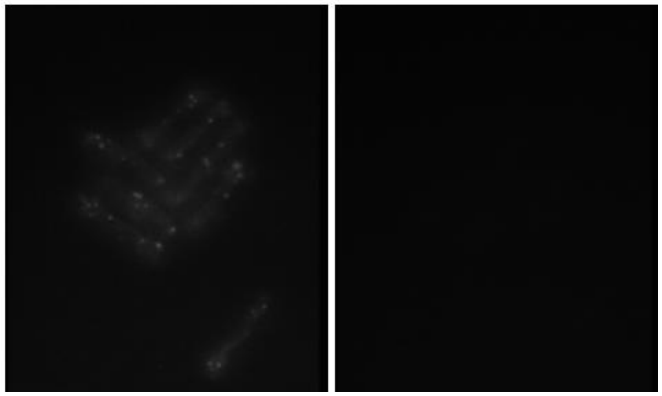

B

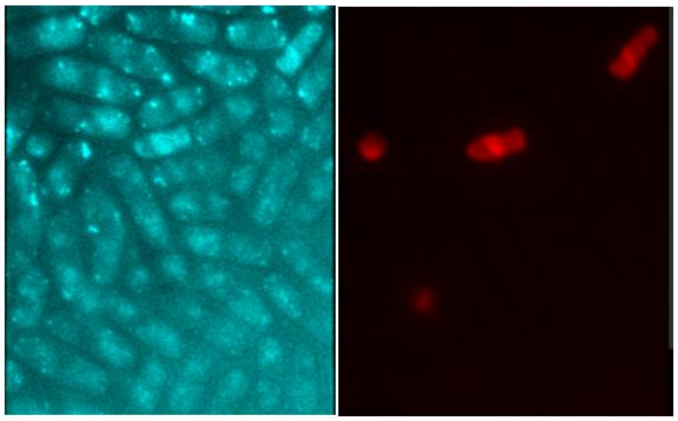

Figure 7. Preliminary results of two-color TIRF imaging system

Left is mEGFP emission channel. Right is SiR647 emission channel.

A: mEGFP-fim1 acp1-SNAP strain imaged with 488nm laser

B: mEGFP-fim1 acp1-SNAP strain imaged with both 488nm and 640nm laser

5 Outlook

Up to now, we investigated the dwell-time distributions of single-molecule endocytic proteins. More specifically, we focused on the proteins related to the actin machinery and provided new understanding of actin crosslinking mechanisms. There is still much potential to use our strategy to better understand the molecular mechanisms of endocytosis.

In this dissertation, we only included two different fim1p truncated constructs (ABD1-ABD2 and ABD2). Single molecule tracking of other fim1p truncated constructs could provide more insights of the function of EH domain.

Since the two-color TIRF imaging system was already built, measuring single molecule motions relative to the endocytic patch would help us understand how endocytic proteins cooperate with each other. For better imaging quality with two-color TIRF, we have tried to fuse Halo-tag to fim1p and label with JF646 and obtained some promising preliminary results. Future two-color imaging experiments can use JF dyes with better brightness and photostability as a substitution of SiR647. However, the steric hindrance of fusing Halo-tag to endocytic proteins needs to be considered, since the size of Halo-tag is about 32 kDa, which is comparable to mEGFP and larger than the SNAP-tag (17.5 kDa)

The dwell-time distributions we obtained for the actin machinery related proteins share the similar shape. Although the Wilcoxon rank sum test showed that the data sets were significantly different, it was hard to tell the difference between them. Future study can take advantage machine learning algorithms. The quantities we measured dwell-time,

displacement per frame, moving distance per frame, velocity in x and y respectively, speed in x and y respectively, fluorescent intensity of each spot in time series, and mean squared displacement. We could use these quantities as features and feed a tree-based model to figure out the feature importance of them. If more data were to be collected in the future, we would also be able to build an artificial neural network model using existing features to predict protein type. In this way, it would be possible for us to know what the significant different features between different endocytic proteins are, which could help us to obtain more intuition of their mechanisms.

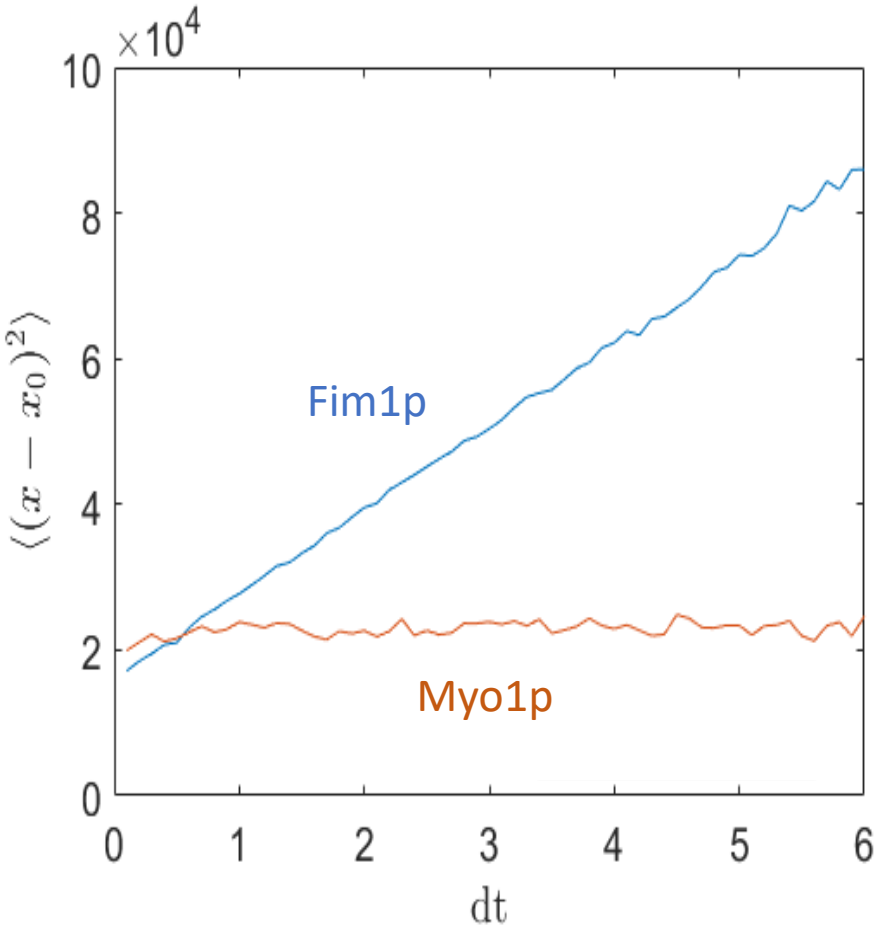

Figure S4. MSD of single molecule myo1p and fim1p

The mean squared displacement (MSD) for fim1p and myo1p are shown as blue and orange. The motion of myo1p is hindered and in a limited region while Fim1p is diffusive.

Appendix 1 Methods and Experimental Design

A 1.1 Strain Construction

For SNAP tagging, we fused a SNAP-tag to endocytic protein of interest by homologous recombination and selection with Kanamycin[85] or by CRISPR-Cas9 and selection with fluoride[16] (Table 1). For *end4* deletion in wild type strains, we used homologous recombination and selection with Kanamycin. For *end4* deletion in fim1-mEGFP strain, we introduced an early stop codon in the early amino acids of the coding sequence of *end4* to stop its expression. For introducing 2A self-cleavage peptide into fim1p genome, we use CRISPR-Cas9 and selection with fluoride.

A 1.2 Labeling for Imaging

We grew our SNAP-tag and mEGFP strains in liquid YE5S medium at 32℃ for 16 hours. For mEGFP strains, we then diluted them into OD 0.1 with EMM5S medium and let them grow for another 16 hours at 25℃. For SNAP-tag strains, after growing in YE5S medium at 32℃ for 16 hours, we diluted them into OD 0.1 with EMM5S medium and let them grow for 8 hours at 25℃ until the OD reaches 0.4-0.6. We then diluted them to OD 0.1 with EMM5S with a final concentration 1μM of silicon-rhodamine benzylguanine derivative SNAP-SiR647[86]. The culture tube used for labeling were wrapped in aluminum foil to avoid the photobleaching of the fluorophore by room light. After overnight labeling (16 hours) at 25℃, the cells were washed 5 times (1500xg, 3min) and incubated at 25℃ for another hour. We then washed the cells for another 5 times (1500xg, 3min) and resuspended them in 50-100μL filtered EMM5S for imaging.

For Halo-tag strains labeled with JF646 dye, we followed the same labeling strategy as discussed above but only incubate the labeling tube for 10 hours. We have found that 16 hours labeling with 1μM of JF646 ended up with over labeling. The concentration of dye could be further tuned to accommodate with longer labeling time.

A 1.3 Single-Color TIRF Imaging

We washed #1.5 coverslips in an ethanol bath for 30mins. We then blew them dry and plasma cleaned them for 3mins. We pipetted 6μL cells onto 25% gelatin pad and covered them with cleaned cover slip. The sample was then sealed with Valap.

We used an Eclipse Ti inverted TIRF microscope with a 60x/1.49 objective, 1.5x magnifying lens and iXon Du897 EMCCD camera. We used 2.5% and 5% 642nm laser (1.2 and 2.1W/cm^2 measured at exiting objective) to image our SNAP-tag strains (with SiR647 dye bind with SNAP-tag) and 488nm laser (0.2W/cm^2 measured at exiting objective) to image our mEGFP strains.

For SNAP-tag strain imaging, the focal plane was set to be 1.5μm below the cell midplane. In this way, the focal plane was close to cell edge so that more endocytic events were collected, and background fluorescence were reduced. The TIRF angle was set to 1170, where near-TIRF illumination (HILO) was achieved. The exposure time was set as 100ms. For each movie we recorded, we first start collecting movies for a few seconds (1-3s) with the laser off. We then turned on the laser and collected movie for 30s.

For mEGFP strain imaging, the exposure time was set to 100ms. For each movie we recorded, we first started collecting movies for a few seconds (1-3s) with the laser off. We then turned on the laser and collected movie for 60s. Longer movie length was

necessary in imaging proteins tagged with a fluorescnt protein compared to single molecule imaging because the patch lifetime of endocytic protein is 20-25 seconds.

A 1.4 Two-Color TIRF Imaging

We washed #1.5 coverslips in an ethanol bath for 30mins. We then blew them dry and plasma cleaned them for 3mins. We pipetted 6μL cells onto 25% gelatin pad and covered them with cleaned cover slip. The sample was then sealed with Valap.

We used a Nikon Ti2 TIRF/STORM system with a quad-band filter (TRF89901) suitable for Gemini W-view system. We first manually installed the quad-band filter. We used fluorescent beads to align 488nm laser (0.2W/cm^2 measured at exiting objective) and 640nm laser (3.5W/cm^2 measured at exiting objective). Since there was a software synchronization issue, we were not able to tune the 640nm laser. The 640nm laser power needed to be tuned further down to achieve better imaging quality.

The focal plane was set to be 1.5μm below the cell midplane. The TIRF angle was set to be 67.4, where perfect TIRF illumination was achieved. The exposure time was set as 100ms. For each movie we recorded, we first turned the 488nm laser on to look for the endocytic patches. We then turned the 640nm laser on for a few seconds and started collecting movie for 60s.

A 1.5 Image analysis

We used Python Microscopy Environment (PYME) for single molecule spot localization. We converted our nd2 imaging file into TIFF file by Fiji ImageJ. A meta file containing camera properties is generated as follows:

md[‘voxelsize.units’] = ‘um’

md[‘voxelsize.x’] = 0.178

md[‘voxelsize.y’] = 0.178

md[‘voxelsize.z’] = 300

md[‘Camera.TrueEMGain’] = 167

md[‘Camera.NoiseFactor’] = 1.41

md[‘Camera.ElectronsPerCount’] = 49

md[‘Camera.ReadNoise’] = 88.8

md[‘Camera.ADOffest’] = 105

md[‘EstimatedLaserOnFrameNo’] = 5

We then ran DH5view to open converted TIFF imaging file. The parameters of spot localization are as follows:

‘Threshold’ : 1.2, which is the ratio between spot and local intensity for spot detection.

‘Debounce rad’ : 3, which is the number of pixel where two spots cannot be separated.

‘Type of fit’: LatGaussFitFR, which is to fit the spot with a 2D Gaussian distribution

‘Start at’: the frame after the laser turned on

‘Subtract Background’: uncheck

After the spot localization, we used VisGUI to filter the spots. In VisGUI, we typed the commands in Python console for spot filtration. The parameters for spot filtration are as follows:

A: 20-200, which is the spot brightness)

Sig: 75-250, which is the standard deviation of the 2D Gaussian)

error_x and error_y: both are 0-150, which are the precisions of fitting in x and y direction

max_gap: 6, which means we allow the two consecutive spots from one trajectory having a maximum gap of 4 frames (6 includes the starting and ending frames where we can detect the spots)

clumpsize: 3, which means the minimum number of spots in one trajectory is 3.

We then used Matlab (MathWorks, Inc) to further analyze the data obtained from PYME analysis. We grouped the spots by their ClumpIndex where different ClumpIndex identified different trajectories. For each trajectory, we calculated the dwell-time (time difference between the frame where the spot was first detected and the frame where the spot was last detected, a maximum gap of 4 frames was allowed), displacement per frame, moving distance per frame, velocity in x and y respectively, speed in x and y respectively, fluorescent intensity of each spot in time series, and mean squared displacement.

Since actin-machinery related proteins had similar looking dwell-time distributions, we applied statistical tests to confirm the differences between their dwell-time distributions. We randomly split the dwell-time data set into 5 subsets and applied Wilcoxon rank sum test between each of them to make sure there was not significant difference detected between each subset. We also applied Wilcoxon rank sum test between different endocytic proteins dwell-time datasets to assure the existing of the significant difference. Usually, the dwell-time data obtained from low quality images would end up with no significant difference between each other.

Table 1. Yeast Strains used in this study

Strain	Genotype	Source
JB135	*fim1-SNAP-kanMX6 ade6-M216 his3-D1 leu1-32 ura4-D18*	(Lacy 2019)[17]
JB216	*41nmt1-SNAP-actin-leu+ ade6-M216 his3-D1 ura4-D19*	(Lacy 2019)[17]
JB304	*SNAP-myo1 fex1Δ fex2Δ ade6-M216 his3-D1 leu1-32 ura4-D18*	(Lacy 2019)[17]
JB305	*acp1-SNAP fex1Δ fex2Δ ade6-M216 his3-D1 leu1-32 ura4-D18*	(Lacy 2019)[17]
JB517	*SNAP-fim1 end4Δ-kanMX6 ade6-M210 his3-D1 leu1-32 ura4-D18*	This study
JB646	*fim1-EF-ERBV-1-20AA-ABD1-ABD2-SNAP fex1Δ fex2Δ ade6-M216 his3-D1 leu1-32 ura4-D18*	This study
JB647	*fim1-EF-ABD1-ERBV1-20AA-ABD2-SNAP fex1Δ fex2Δ ade6-M216 his3-D1 leu1-32 ura4-D18*	This study

References

(1) Doherty, G. J.; McMahon, H. T. Mechanisms of Endocytosis. *Annu Rev Biochem* **2009**, *78*, 857–902. https://doi.org/10.1146/annurev.biochem.78.081307.110540.

(2) Boettner, D. R.; Chi, R. J.; Lemmon, S. K. Lessons from Yeast for Clathrin-Mediated Endocytosis. *Nature Cell Biology* **2012**, *14* (1), 2–10. https://doi.org/10.1038/ncb2403.

(3) Taylor, M. J.; Perrais, D.; Merrifield, C. J. A High Precision Survey of the Molecular Dynamics of Mammalian Clathrin-Mediated Endocytosis. *PLoS Biol* **2011**, *9* (3), e1000604–e1000604. https://doi.org/10.1371/journal.pbio.1000604.

(4) McMahon, H. T.; Boucrot, E. Molecular Mechanism and Physiological Functions of Clathrin-Mediated Endocytosis. *Nature Reviews Molecular Cell Biology* **2011**, *12* (8), 517–533. https://doi.org/10.1038/nrm3151.

(5) ROSENBLUTH, J.; WISSIG, S. L. THE DISTRIBUTION OF EXOGENOUS FERRITIN IN TOAD SPINAL GANGLIA AND THE MECHANISM OF ITS UPTAKE BY NEURONS. *J Cell Biol* **1964**, *23* (2), 307–325. https://doi.org/10.1083/jcb.23.2.307.

(6) von Zastrow, M.; Williams, J. T. Modulating Neuromodulation by Receptor Membrane Traffic in the Endocytic Pathway. *Neuron* **2012**, *76* (1), 22–32. https://doi.org/10.1016/j.neuron.2012.09.022.

(7) Merrifield, C. J.; Kaksonen, M. Endocytic Accessory Factors and Regulation of Clathrin-Mediated Endocytosis. *Cold Spring Harb Perspect Biol* **2014**, *6* (11), a016733–a016733. https://doi.org/10.1101/cshperspect.a016733.

(8) Mooren, O. L.; Galletta, B. J.; Cooper, J. A. Roles for Actin Assembly in Endocytosis. *Annu Rev Biochem* **2012**, *81*, 661–686. https://doi.org/10.1146/annurev-biochem-060910-094416.

(9) Prescianotto-Baschong, C.; Riezman, H. Morphology of the Yeast Endocytic Pathway. *Mol Biol Cell* **1998**, *9* (1), 173–189. https://doi.org/10.1091/mbc.9.1.173.

(10) Kaksonen, M.; Roux, A. Mechanisms of Clathrin-Mediated Endocytosis. *Nat Rev Mol Cell Biol* **2018**, *19* (5), 313–326. https://doi.org/10.1038/nrm.2017.132.

(11) Kumari, S.; MG, S.; Mayor, S. Endocytosis Unplugged: Multiple Ways to Enter the Cell. *Cell Research* **2010**, *20* (3), 256–275. https://doi.org/10.1038/cr.2010.19.

(12) Parkar, N. S.; Akpa, B. S.; Nitsche, L. C.; Wedgewood, L. E.; Place, A. T.; Sverdlov, M. S.; Chaga, O.; Minshall, R. D. Vesicle Formation and Endocytosis: Function, Machinery, Mechanisms, and Modeling. *Antioxid Redox Signal* **2009**, *11* (6), 1301–1312. https://doi.org/10.1089/ars.2008.2397.

(13) Lampe, M.; Vassilopoulos, S.; Merrifield, C. Clathrin Coated Pits, Plaques and Adhesion. *Journal of Structural Biology* **2016**, *196* (1), 48–56. https://doi.org/10.1016/j.jsb.2016.07.009.

(14) Perrais, D.; Merrifield, C. J. Dynamics of Endocytic Vesicle Creation. *Developmental Cell* **2005**, *9* (5), 581–592. https://doi.org/10.1016/j.devcel.2005.10.002.

(15) Petersen, J.; Russell, P. Growth and the Environment of Schizosaccharomyces Pombe. *Cold Spring Harb Protoc* **2016**, *2016* (3), pdb.top079764-pdb.top079764. https://doi.org/10.1101/pdb.top079764.

(16) Fernandez, R.; Berro, J. Use of a Fluoride Channel as a New Selection Marker for Fission Yeast Plasmids and Application to Fast Genome Editing with CRISPR/Cas9. *Yeast* **2016**, *33* (10), 549–557. https://doi.org/10.1002/yea.3178.

(17) Lacy, M. M.; Baddeley, D.; Berro, J. Single-Molecule Turnover Dynamics of Actin and Membrane Coat Proteins in Clathrin-Mediated Endocytosis. *Elife* **2019**, *8*. https://doi.org/10.7554/eLife.52355.

(18) Grove, J.; Metcalf, D. J.; Knight, A. E.; Wavre-Shapton, S. T.; Sun, T.; Protonotarios, E. D.; Griffin, L. D.; Lippincott-Schwartz, J.; Marsh, M. Flat Clathrin Lattices: Stable Features of the Plasma Membrane. *Mol Biol Cell* **2014**, *25* (22), 3581–3594. https://doi.org/10.1091/mbc.E14-06-1154.

(19) Iwaki, T.; Tanaka, N.; Takagi, H.; Giga-Hama, Y.; Takegawa, K. Characterization of End4+, a Gene Required for Endocytosis in Schizosaccharomyces Pombe. *Yeast* **2004**, *21* (10), 867–881. https://doi.org/10.1002/yea.1134.

(20) Weinberg, J.; Drubin, D. G. Clathrin-Mediated Endocytosis in Budding Yeast. *Trends Cell Biol* **2012**, *22* (1), 1–13. https://doi.org/10.1016/j.tcb.2011.09.001.

(21) Dannhauser, P. N.; Ungewickell, E. J. Reconstitution of Clathrin-Coated Bud and Vesicle Formation with Minimal Components. *Nat Cell Biol* **2012**, *14* (6), 634–639. https://doi.org/10.1038/ncb2478.

(22) Boulant, S.; Kural, C.; Zeeh, J.-C.; Ubelmann, F.; Kirchhausen, T. Actin Dynamics Counteract Membrane Tension during Clathrin-Mediated Endocytosis. *Nat Cell Biol* **2011**, *13* (9), 1124–1131. https://doi.org/10.1038/ncb2307.

(23) Kukulski, W.; Schorb, M.; Kaksonen, M.; Briggs, J. A. G. Plasma Membrane Reshaping during Endocytosis Is Revealed by Time-Resolved Electron Tomography. *Cell* **2012**, *150* (3), 508–520. https://doi.org/10.1016/j.cell.2012.05.046.

(24) Sun, Y.; Martin, A. C.; Drubin, D. G. Endocytic Internalization in Budding Yeast Requires Coordinated Actin Nucleation and Myosin Motor Activity. *Developmental Cell* **2006**, *11* (1), 33–46. https://doi.org/10.1016/j.devcel.2006.05.008.

(25) Picco, A.; Mund, M.; Ries, J.; Nédélec, F.; Kaksonen, M. Visualizing the Functional Architecture of the Endocytic Machinery. *eLife* **2015**, *4*, e04535. https://doi.org/10.7554/eLife.04535.

(26) Berro, J.; Pollard, T. D. Local and Global Analysis of Endocytic Patch Dynamics in Fission Yeast Using a New "Temporal Superresolution" Realignment Method. *Mol Biol Cell* **2014**, *25* (22), 3501–3514. https://doi.org/10.1091/mbc.E13-01-0004.

(27) Sirotkin, V.; Berro, J.; Macmillan, K.; Zhao, L.; Pollard, T. D. Quantitative Analysis of the Mechanism of Endocytic Actin Patch Assembly and Disassembly in Fission Yeast. *Mol Biol Cell* **2010**, *21* (16), 2894–2904. https://doi.org/10.1091/mbc.E10-02-0157.

(28) Berro, J.; Sirotkin, V.; Pollard, T. D. Mathematical Modeling of Endocytic Actin Patch Kinetics in Fission Yeast: Disassembly Requires Release of Actin Filament Fragments. *Mol Biol Cell* **2010**, *21* (16), 2905–2915. https://doi.org/10.1091/mbc.E10-06-0494.

(29) Klein, M. G.; Shi, W.; Ramagopal, U.; Tseng, Y.; Wirtz, D.; Kovar, D. R.; Staiger, C. J.; Almo, S. C. Structure of the Actin Crosslinking Core of Fimbrin. *Structure* **2004**, *12* (6), 999–1013. https://doi.org/10.1016/j.str.2004.04.010.

(30) Goode, B. L.; Eskin, J. A.; Wendland, B. Actin and Endocytosis in Budding Yeast. *Genetics* **2015**, *199* (2), 315–358. https://doi.org/10.1534/genetics.112.145540.

(31) Skau, C. T.; Courson, D. S.; Bestul, A. J.; Winkelman, J. D.; Rock, R. S.; Sirotkin, V.; Kovar, D. R. Actin Filament Bundling by Fimbrin Is Important for Endocytosis, Cytokinesis, and Polarization in Fission Yeast. *J Biol Chem* **2011**, *286* (30), 26964–26977. https://doi.org/10.1074/jbc.M111.239004.

(32) Christensen, J. R.; Hocky, G. M.; Homa, K. E.; Morganthaler, A. N.; Hitchcock-DeGregori, S. E.; Voth, G. A.; Kovar, D. R. Competition between Tropomyosin, Fimbrin, and ADF/Cofilin Drives Their Sorting to Distinct Actin Filament Networks. *Elife* **2017**, *6*. https://doi.org/10.7554/eLife.23152.

(33) Skau, C. T.; Kovar, D. R. Fimbrin and Tropomyosin Competition Regulates Endocytosis and Cytokinesis Kinetics in Fission Yeast. *Curr Biol* **2010**, *20* (16), 1415–1422. https://doi.org/10.1016/j.cub.2010.06.020.

(34) Christensen, J. R.; Homa, K. E.; Morganthaler, A. N.; Brown, R. R.; Suarez, C.; Harker, A. J.; O'Connell, M. E.; Kovar, D. R. Cooperation between Tropomyosin and α-Actinin Inhibits Fimbrin Association with Actin Filament Networks in Fission Yeast. *Elife* **2019**, *8*. https://doi.org/10.7554/eLife.47279.

(35) Reis, C. R.; Chen, P.-H.; Srinivasan, S.; Aguet, F.; Mettlen, M.; Schmid, S. L. Crosstalk between Akt/GSK3β Signaling and Dynamin-1 Regulates Clathrin-Mediated Endocytosis. *EMBO J* **2015**, *34* (16), 2132–2146. https://doi.org/10.15252/embj.201591518.

(36) Podh, N. K.; Paliwal, S.; Dey, P.; Das, A.; Morjaria, S.; Mehta, G. In-Vivo Single-Molecule Imaging in Yeast: Applications and Challenges. *J Mol Biol* **2021**, *433* (22), 167250. https://doi.org/10.1016/j.jmb.2021.167250.

(37) Kusumi, A.; Tsunoyama, T. A.; Hirosawa, K. M.; Kasai, R. S.; Fujiwara, T. K. Tracking Single Molecules at Work in Living Cells. *Nature Chemical Biology* **2014**, *10* (7), 524–532. https://doi.org/10.1038/nchembio.1558.

(38) Xia, T.; Li, N.; Fang, X. Single-Molecule Fluorescence Imaging in Living Cells. *Annu Rev Phys Chem* **2013**, *64*, 459–480. https://doi.org/10.1146/annurev-physchem-040412-110127.

(39) Luo, F.; Qin, G.; Xia, T.; Fang, X. Single-Molecule Imaging of Protein Interactions and Dynamics. *Annu Rev Anal Chem (Palo Alto Calif)* **2020**, *13* (1), 337–361. https://doi.org/10.1146/annurev-anchem-091619-094308.

(40) Schmidt, A.; Gao, G.; Little, S. R.; Jalihal, A. P.; Walter, N. G. Following the Messenger: Recent Innovations in Live Cell Single Molecule Fluorescence Imaging. *Wiley Interdiscip Rev RNA* **2020**, *11* (4), e1587. https://doi.org/10.1002/wrna.1587.

(41) Ananthanarayanan, V.; Schattat, M.; Vogel, S. K.; Krull, A.; Pavin, N.; Tolić-Nørrelykke, I. M. Dynein Motion Switches from Diffusive to Directed upon Cortical Anchoring. *Cell* **2013**, *153* (7), 1526–1536. https://doi.org/10.1016/j.cell.2013.05.020.

(42) Botman, D.; de Groot, D. H.; Schmidt, P.; Goedhart, J.; Teusink, B. In Vivo Characterisation of Fluorescent Proteins in Budding Yeast. *Scientific Reports* **2019**, *9* (1), 2234. https://doi.org/10.1038/s41598-019-38913-z.

(43) Hess, S. T.; Girirajan, T. P. K.; Mason, M. D. Ultra-High Resolution Imaging by Fluorescence Photoactivation Localization Microscopy. *Biophys J* **2006**, *91* (11), 4258–4272. https://doi.org/10.1529/biophysj.106.091116.

(44) Wu, X.-S.; Lee, S. H.; Sheng, J.; Zhang, Z.; Zhao, W.-D.; Wang, D.; Jin, Y.; Charnay, P.; Ervasti, J. M.; Wu, L.-G. Actin Is Crucial for All Kinetically Distinguishable Forms of Endocytosis at Synapses. *Neuron* **2016**, *92* (5), 1020–1035. https://doi.org/10.1016/j.neuron.2016.10.014.

(45) Wu, J.-Q.; Pollard, T. D. Counting Cytokinesis Proteins Globally and Locally in Fission Yeast. *Science* **2005**, *310* (5746), 310–314. https://doi.org/10.1126/science.1113230.

(46) Thorn, K. Genetically Encoded Fluorescent Tags. *Mol Biol Cell* **2017**, *28* (7), 848–857. https://doi.org/10.1091/mbc.E16-07-0504.

(47) Wurm, C. A.; Suppanz, I. E.; Stoldt, S.; Jakobs, S. Rapid FlAsH Labelling in the Budding Yeast Saccharomyces Cerevisiae. *J Microsc* **2010**, *240* (1), 6–13. https://doi.org/10.1111/j.1365-2818.2010.03378.x.

(48) Gautier, A.; Juillerat, A.; Heinis, C.; Corrêa, I. R.; Kindermann, M.; Beaufils, F.; Johnsson, K. An Engineered Protein Tag for Multiprotein Labeling in Living Cells. *Chemistry & Biology* **2008**, *15* (2), 128–136. https://doi.org/10.1016/j.chembiol.2008.01.007.

(49) Los, G. V.; Encell, L. P.; McDougall, M. G.; Hartzell, D. D.; Karassina, N.; Zimprich, C.; Wood, M. G.; Learish, R.; Ohana, R. F.; Urh, M.; Simpson, D.; Mendez, J.; Zimmerman, K.; Otto, P.; Vidugiris, G.; Zhu, J.; Darzins, A.; Klaubert, D. H.; Bulleit, R. F.; Wood, K. V. HaloTag: A Novel Protein Labeling Technology for Cell Imaging and Protein Analysis. *ACS Chem. Biol.* **2008**, *3* (6), 373–382. https://doi.org/10.1021/cb800025k.

(50) Juillerat, A.; Gronemeyer, T.; Keppler, A.; Gendreizig, S.; Pick, H.; Vogel, H.; Johnsson, K. Directed Evolution of O6-Alkylguanine-DNA Alkyltransferase for Efficient Labeling of Fusion

Proteins with Small Molecules In Vivo. *Chemistry & Biology* **2003**, *10* (4), 313–317. https://doi.org/10.1016/S1074-5521(03)00068-1.

(51) Yaffe, M. P.; Stuurman, N.; Vale, R. D. Mitochondrial Positioning in Fission Yeast Is Driven by Association with Dynamic Microtubules and Mitotic Spindle Poles. *Proc Natl Acad Sci U S A* **2003**, *100* (20), 11424–11428. https://doi.org/10.1073/pnas.1534703100.

(52) Spira, F.; Dominguez-Escobar, J.; Müller, N.; Wedlich-Söldner, R. Visualization of Cortex Organization and Dynamics in Microorganisms, Using Total Internal Reflection Fluorescence Microscopy. *J Vis Exp* **2012**, No. 63, e3982–e3982. https://doi.org/10.3791/3982.

(53) Fish, K. N. Total Internal Reflection Fluorescence (TIRF) Microscopy. *Curr Protoc Cytom* **2009**, *Chapter 12*, Unit12.18. https://doi.org/10.1002/0471142956.cy1218s50.

(54) Axelrod, D. Cell-Substrate Contacts Illuminated by Total Internal Reflection Fluorescence. *J Cell Biol* **1981**, *89* (1), 141–145. https://doi.org/10.1083/jcb.89.1.141.

(55) Stout, A. L.; Axelrod, D. Evanescent Field Excitation of Fluorescence by Epi-Illumination Microscopy. *Appl. Opt.* **1989**, *28* (24), 5237–5242. https://doi.org/10.1364/AO.28.005237.

(56) Martin-Fernandez, M. L.; Tynan, C. J.; Webb, S. E. D. A "pocket Guide" to Total Internal Reflection Fluorescence. *J Microsc* **2013**, *252* (1), 16–22. https://doi.org/10.1111/jmi.12070.

(57) Tokunaga, M.; Imamoto, N.; Sakata-Sogawa, K. Highly Inclined Thin Illumination Enables Clear Single-Molecule Imaging in Cells. *Nature Methods* **2008**, *5* (2), 159–161. https://doi.org/10.1038/nmeth1171.

(58) Shashkova, S.; Andersson, M.; Hohmann, S.; Leake, M. C. Correlating Single-Molecule Characteristics of the Yeast Aquaglyceroporin Fps1 with Environmental Perturbations Directly in Living Cells. *Methods* **2021**, *193*, 46–53. https://doi.org/10.1016/j.ymeth.2020.05.003.

(59) Wollman, A. J. M.; Leake, M. C. Single-Molecule Narrow-Field Microscopy of Protein–DNA Binding Dynamics in Glucose Signal Transduction of Live Yeast Cells. In *Chromosome Architecture: Methods and Protocols*; Leake, M. C., Ed.; Springer New York: New York, NY, 2016; pp 5–15. https://doi.org/10.1007/978-1-4939-3631-1_2.

(60) Plank, M.; Wadhams, G. H.; Leake, M. C. Millisecond Timescale Slimfield Imaging and Automated Quantification of Single Fluorescent Protein Molecules for Use in Probing Complex Biological Processes. *Integrative Biology* **2009**, *1* (10), 602–612. https://doi.org/10.1039/b907837a.

(61) Vettenburg, T.; Dalgarno, H. I. C.; Nylk, J.; Coll-Lladó, C.; Ferrier, D. E. K.; Čižmár, T.; Gunn-Moore, F. J.; Dholakia, K. Light-Sheet Microscopy Using an Airy Beam. *Nature Methods* **2014**, *11* (5), 541–544. https://doi.org/10.1038/nmeth.2922.

(62) Gao, L.; Shao, L.; Chen, B.-C.; Betzig, E. 3D Live Fluorescence Imaging of Cellular Dynamics Using Bessel Beam Plane Illumination Microscopy. *Nature Protocols* **2014**, *9* (5), 1083–1101. https://doi.org/10.1038/nprot.2014.087.

(63) Lu, C.-H.; Tang, W.-C.; Liu, Y.-T.; Chang, S.-W.; Wu, F. C. M.; Chen, C.-Y.; Tsai, Y.-C.; Yang, S.-M.; Kuo, C.-W.; Okada, Y.; Hwu, Y.-K.; Chen, P.; Chen, B.-C. Lightsheet Localization Microscopy Enables Fast, Large-Scale, and Three-Dimensional Super-Resolution Imaging. *Communications Biology* **2019**, *2* (1), 177. https://doi.org/10.1038/s42003-019-0403-9.

(64) Wu, Y.; Kumar, A.; Smith, C.; Ardiel, E.; Chandris, P.; Christensen, R.; Rey-Suarez, I.; Guo, M.; Vishwasrao, H. D.; Chen, J.; Tang, J.; Upadhyaya, A.; La Riviere, P. J.; Shroff, H. Reflective Imaging Improves Spatiotemporal Resolution and Collection Efficiency in Light Sheet Microscopy. *Nature Communications* **2017**, *8* (1), 1452. https://doi.org/10.1038/s41467-017-01250-8.

(65) Su, L.; Lu, G.; Kenens, B.; Rocha, S.; Fron, E.; Yuan, H.; Chen, C.; Van Dorpe, P.; Roeffaers, M. B. J.; Mizuno, H.; Hofkens, J.; Hutchison, J. A.; Uji-I, H. Visualization of Molecular Fluorescence Point Spread Functions via Remote Excitation Switching Fluorescence Microscopy. *Nat Commun* **2015**, *6*, 6287. https://doi.org/10.1038/ncomms7287.

(66) Mortensen, K. I.; Churchman, L. S.; Spudich, J. A.; Flyvbjerg, H. Optimized Localization Analysis for Single-Molecule Tracking and Super-Resolution Microscopy. *Nat Methods* **2010**, *7* (5), 377–381. https://doi.org/10.1038/nmeth.1447.

(67) Yang, L.; Parton, R.; Ball, G.; Qiu, Z.; Greenaway, A. H.; Davis, I.; Lu, W. An Adaptive Non-Local Means Filter for Denoising Live-Cell Images and Improving Particle Detection. *Journal of Structural Biology* **2010**, *172* (3), 233–243. https://doi.org/10.1016/j.jsb.2010.06.019.

(68) Smith, C. S.; Stallinga, S.; Lidke, K. A.; Rieger, B.; Grunwald, D. Probability-Based Particle Detection That Enables Threshold-Free and Robust in Vivo Single-Molecule Tracking. *MBoC* **2015**, *26* (22), 4057–4062. https://doi.org/10.1091/mbc.E15-06-0448.

(69) Oheim, M.; Salomon, A.; Weissman, A.; Brunstein, M.; Becherer, U. Calibrating Evanescent-Wave Penetration Depths for Biological TIRF Microscopy. *Biophysical Journal* **2019**, *117* (5), 795–809. https://doi.org/10.1016/j.bpj.2019.07.048.

(70) Jaqaman, K.; Loerke, D.; Mettlen, M.; Kuwata, H.; Grinstein, S.; Schmid, S. L.; Danuser, G. Robust Single-Particle Tracking in Live-Cell Time-Lapse Sequences. *Nature Methods* **2008**, *5* (8), 695–702. https://doi.org/10.1038/nmeth.1237.

(71) Lacy, M. M.; Baddeley, D.; Berro, J. Single-Molecule Imaging of the BAR-Domain Protein Pil1p Reveals Filament-End Dynamics. *Mol Biol Cell* **2017**, *28* (17), 2251–2259. https://doi.org/10.1091/mbc.E17-04-0238.

(72) Meijering, E.; Dzyubachyk, O.; Smal, I. Methods for Cell and Particle Tracking. *Methods Enzymol* **2012**, *504*, 183–200. https://doi.org/10.1016/B978-0-12-391857-4.00009-4.

(73) Kuhn, T.; Hettich, J.; Davtyan, R.; Gebhardt, J. C. M. Single Molecule Tracking and Analysis Framework Including Theory-Predicted Parameter Settings. *Scientific Reports* **2021**, *11* (1), 9465. https://doi.org/10.1038/s41598-021-88802-7.

(74) Michalet, X. Mean Square Displacement Analysis of Single-Particle Trajectories with Localization Error: Brownian Motion in an Isotropic Medium. *Phys Rev E Stat Nonlin Soft Matter Phys* **2010**, *82* (4 Pt 1), 041914–041914. https://doi.org/10.1103/PhysRevE.82.041914.

(75) Ernst, D.; Köhler, J. Measuring a Diffusion Coefficient by Single-Particle Tracking: Statistical Analysis of Experimental Mean Squared Displacement Curves. *Phys. Chem. Chem. Phys.* **2013**, *15* (3), 845–849. https://doi.org/10.1039/C2CP43433D.

(76) Persson, F.; Lindén, M.; Unoson, C.; Elf, J. Extracting Intracellular Diffusive States and Transition Rates from Single-Molecule Tracking Data. *Nature Methods* **2013**, *10* (3), 265–269. https://doi.org/10.1038/nmeth.2367.

(77) Chen, Z.; Geffroy, L.; Biteen, J. S. NOBIAS: Analyzing Anomalous Diffusion in Single-Molecule Tracks With Nonparametric Bayesian Inference. *Frontiers in Bioinformatics* **2021**, *1*, 40. https://doi.org/10.3389/fbinf.2021.742073.

(78) Lindén, M.; Elf, J. Variational Algorithms for Analyzing Noisy Multistate Diffusion Trajectories. *Biophys J* **2018**, *115* (2), 276–282. https://doi.org/10.1016/j.bpj.2018.05.027.

(79) Falcao, R. C.; Coombs, D. Diffusion Analysis of Single Particle Trajectories in a Bayesian Nonparametrics Framework. *Phys Biol* **2020**, *17* (2), 025001. https://doi.org/10.1088/1478-3975/ab64b3.

(80) Dmitrieff, S.; Nédélec, F. Membrane Mechanics of Endocytosis in Cells with Turgor. *PLOS Computational Biology* **2015**, *11* (10), e1004538. https://doi.org/10.1371/journal.pcbi.1004538.

(81) Tweten, D. J.; Bayly, P. V.; Carlsson, A. E. Actin Growth Profile in Clathrin-Mediated Endocytosis. *Phys. Rev. E* **2017**, *95* (5), 052414. https://doi.org/10.1103/PhysRevE.95.052414.

(82) Ma, R.; Berro, J. Structural Organization and Energy Storage in Crosslinked Actin Assemblies. *PLoS Comput Biol* **2018**, *14* (5), e1006150. https://doi.org/10.1371/journal.pcbi.1006150.

(83) Arasada, R.; Sayyad, W. A.; Berro, J.; Pollard, T. D. High-Speed Superresolution Imaging of the Proteins in Fission Yeast Clathrin-Mediated Endocytic Actin Patches. *Mol Biol Cell* **2018**, *29* (3), 295–303. https://doi.org/10.1091/mbc.E17-06-0415.

(84) Lukinavičius, G.; Reymond, L.; Johnsson, K. Fluorescent Labeling of SNAP-Tagged Proteins in Cells. *Methods Mol Biol* **2015**, *1266*, 107–118. https://doi.org/10.1007/978-1-4939-2272-7_7.

(85) Bähler, J.; Wu, J. Q.; Longtine, M. S.; Shah, N. G.; McKenzie, A. 3rd; Steever, A. B.; Wach, A.; Philippsen, P.; Pringle, J. R. Heterologous Modules for Efficient and Versatile PCR-Based Gene Targeting in Schizosaccharomyces Pombe. *Yeast* **1998**, *14* (10), 943–951. https://doi.org/10.1002/(SICI)1097-0061(199807)14:10<943::AID-YEA292>3.0.CO;2-Y.

(86) Keppler, A.; Gendreizig, S.; Gronemeyer, T.; Pick, H.; Vogel, H.; Johnsson, K. *A General Method for the Covalent Labeling of Fusion Proteins with Small Molecules in Vivo.*; United States, 2003; pp 86–89. https://doi.org/10.1038/nbt765.